Eur. Phys. J. D **23**, 25–34 (2003)
DOI: 10.1140/epjd/e2003-00023-y

THE EUROPEAN PHYSICAL JOURNAL D

Stern Gerlach interferometry with metastable argon atoms: an immaterial mask modulating the profile of a supersonic beam

B. Viaris de Lesegno[1], J.C. Karam[2], M. Boustimi[3], F. Perales[2,a], C. Mainos[2], J. Reinhardt[2], J. Baudon[2], V. Bocvarski[4], D. Grancharova[2], F. Pereira Dos Santos[5], T. Durt[2,6], H. Haberland[7], and J. Robert[2]

[1] LCAR-IRSAMC, Université Toulouse 3, Bâtiment 3R1 B4, 118 route de Narbonne, 31062 Toulouse Cedex, France
[2] Laboratoire de Physique des Lasers[b], Université Paris 13, avenue J.B. Clément, 93430 Villetaneuse, France
[3] Laboratoire d'Optronique, ENSSAT, 6 rue de Kérampon, B.P. 447, 22305 Lannion Cedex, France
[4] Institute of Physics, Pregrevica 118, P.O. Box 68, 11080 Zemun, Yugoslavia
[5] Laboratoire Kastler-Brossel, 24 rue Lhomond, 75231 Paris Cedex 05, France
[6] TENA-TONA, Vrije Universiteit Brussel, Pleinlaan 2, 1050 Brussels, Belgium
[7] Universität Freiburg, Hermann-Herder-Strasse 3, 79104 Freiburg, Germany

Received 27 June 2002 / Received in final form 20 September 2002
Published online 4 February 2003 –

Abstract. A new Stern Gerlach interferometer operating with a nozzle beam of metastable argon atoms Ar^* ($3p^5$ $4s$, $^3P_2$) is described. The selection of incoming (polarisation) and outgoing (analysis) Zeeman sublevels is achieved by use of laser induced transitions at two wavelengths, 811.5 nm (closed $J = 2 \rightarrow J = 3$ transition) and 801.5 nm (open $J = 2 \rightarrow J = 2$ transition). Linear superpositions of Zeeman sublevels, just beyond the polariser and just before the analyser, are prepared by means of two zones where Majorana transitions take place. In between, a controlled magnetic field configuration (the phase object) is produced within a triple μ-metal shielding. Standard interference patterns are obtained by scanning the field and detecting the atoms by secondary electron emission from a Faraday cup. When a static radial magnetic gradient is used, the beam profile is modulated by interference. The transverse pattern, which can be translated at will by adding a homogeneous field, is observed for the first time using a multi-channel electron multiplier followed by a phosphor screen and a CCD camera. The results satisfactorily agree with all theoretical predictions.

PACS. 03.75.-b Matter waves – 03.75.Be Atom and neutron optics – 03.75.Dg Atom and neutron interferometry 39.25.+k Atom manipulation (scanning probe microscopy, laser cooling, etc.)

1 Introduction

In the historic Stern Gerlach experiment, magnetic atoms are differently deflected according to the projection of their moment along the direction of the magnetic gradient. This experiment involves an incoherent mixture of atoms (no interference) but it can be considered as the first attempt to exhibit at a macroscopic scale the effect of the field configuration on an atomic beam profile. The fundamental importance of such transverse effects has been recognized for a while by theoreticians [1–3]. On the other hand Stern-Gerlach interferometry (SGI) has proven its ability to manipulate, in a non-trivial manner, through the phaseshifts among different Zeeman sublevels, a beam of atoms having a magnetic moment [4]. Up to now, in such experiments, interferometric effects have been observed on the total outgoing atomic flux, without entering the detail of the density flux profile. The motivation of the present paper is to show how, owing to special properties of rare gas metastable atoms, SGI and imaging techniques in the transverse plane can be combined to obtain new physical insights as well as technical applications.

This polarisation interferometry requires a preparation of the beam in a spin eigenstate usually done without affecting the atom trajectories. However, the beam could be shaped, in a controlled way, previous or during polarisation, *e.g.* by transverse cooling [5]. This would improve older results on atomic diffraction expected to be very sensitive to the macroscopic diaphragms of the interferometer set with a radial gradient of magnetic field [6].

The Majorana transition [7] or "spin flipping" of the polarised beam, yields a linear superposition of Zeeman states. A magnetic profile confined in a macroscopic region along the path of the atoms, forms the heart of the interferometer and creates the different "optical paths" or arms of the interferometer. As a general fact, the classical external motion of the atomic centre of mass is not

[a] e-mail: perales@lpl.univ-paris13.fr
[b] UMR 7538 du CNRS

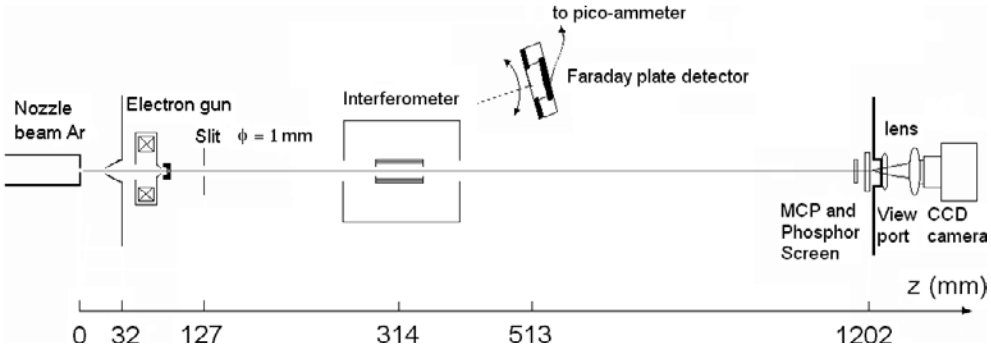

Fig. 1. General scheme of the experimental set up. Distances from the nozzle source are indicated.

affected in this type of interferometer. Nevertheless, it will be shown in this paper that longitudinal and transversal modulations in the density profile of a supersonic beam of metastable argon atoms result from interference.

The experimental study of a new Stern Gerlach interferometer [8] using a supersonic beam of metastable argon atoms (Ar^* $^3P_2$) is the subject of this paper. Our experimental set-up is described in Section 2. We present first the characteristics of the atomic beam and its detection. Details are given for our laser configuration, using two diode lasers to polarise and analyse the Ar^* beam. Finally the interferometer is described in its different parts. In Section 3, we give the results obtained for two configurations of static magnetic fields: a transverse uniform field and a transverse radial gradient field. Conclusions are given in Section 4.

2 Experiment

2.1 Supersonic beam and detection

A continuous supersonic argon beam is excited beyond a skimmer by an anti-parallel electron gun producing a high flux of metastable argon atoms [9] in the $^3P_0$ (11.71 eV) and $^3P_2$ (11.54 eV) states. In our experiment $^3P_0$ atoms (one sixth of the total metastable flux according to the Zeeman degeneracy) contribute as a background signal since they do not possess any magnetic moment. Nevertheless, these atoms could be de-excited to the ground state by the use of a proper diode laser beam ($\lambda = 795$ nm). Time-of-flight measurements using the electron gun with a pulsed accelerating voltage give a Gaussian velocity distribution with an average velocity of 545 m/s and a half width of 44 m/s ($\Delta v/v \sim 8\%$). These results are in good agreement with previous measurements carried out with a slotted disk chopper [9]. In experiments with Ar (5%) seeded in hydrogen (95%) an average velocity of 1 650 m/s with the same resolution is achieved with comparable fluxes. The angular divergence of the supersonic beam is about 8 mrad when a circular aperture (1 mm in diameter) is placed after the electron gun (Fig. 1).

A Faraday cup detector, consisting of a stainless steel disk of diameter 10-mm is connected to a pico-ammeter. A polarised ring helps to extract the Auger emission electrons produced at the surface when metastable argon atoms hit the disk. This allows a measurement of an absolute flux of the full beam (4 mm in diameter at the Faraday disk), through the positive current indicated by the pico-ammeter. Typical currents are in the range 0.1 to 2 nA depending on the electron gun settings, thus giving fluxes in the 10^{10} atoms/s range (*i.e.* 10^{14} at/s/sr). When this global detector is moved out of the beam, a position sensitive detector composed by a micro-channel-plate electron multiplier followed by a phosphor screen detects the beam. An interfaced CCD camera outside the vacuum chamber then records transverse profile images.

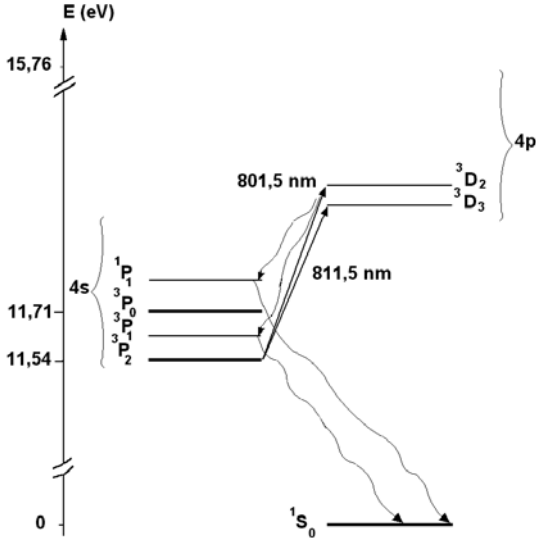

Fig. 2. Energy levels of argon atom involved in this experiment. Long-lived levels (ground-state and metastable states) are indicated by bold lines. Undulating lines show spontaneous decay. The ionisation limit is 15.76 eV.

2.2 Laser system

The wavelengths chosen for the purpose of spin polarisation and analysis of the $^3P_2$ state of a metastable argon atom in the interferometer are respectively 811.5 nm and 801.5 nm (Fig. 2).

Two diode lasers are used in comparable set-ups (Fig. 3). The scheme is the following. A laser diode working at low power (10 to 15 mW) is mounted in a Littrow

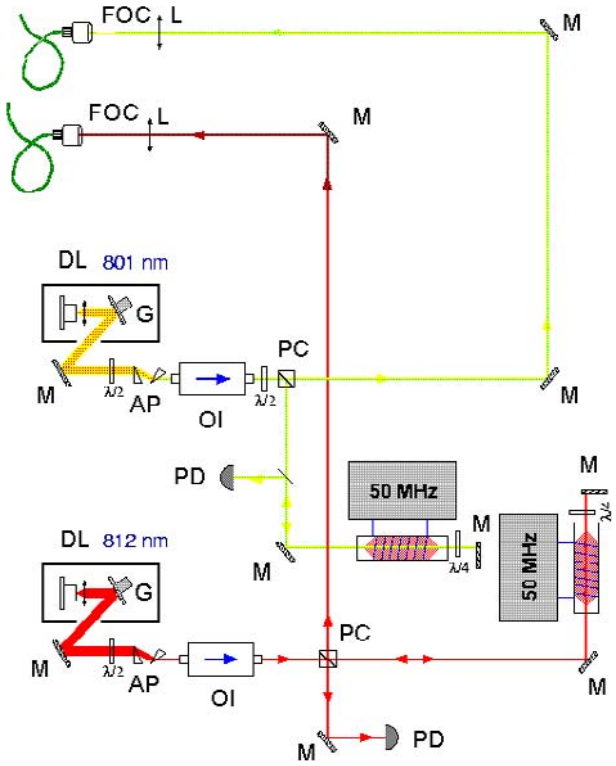

Fig. 3. Lasers system. DL: diode laser and associated collimating optics, G: grating on piezo-ceramic, M: mirror, AP: anamorphic prisms, OI: optical isolator, PC: polarising cube, PD: photodiode, L: lens, FOC: fiber optics coupling.

type extended cavity: a reflection grating (1 200 lines/mm, blazing angle 27°) acts as both the end mirror of the cavity and the dispersion element according to the incidence angle. A piezo-electric ceramic on which the grating is mounted allows for fine-tuning of the frequency as well as for cavity stability when a retroaction signal on the reference atomic line is applied. After crossing a half-wave plate, the laser beam is shaped in a small circular form by passing a pair of anamorphic prisms at Brewster incidence. An optical isolator is used to prevent back reflections. One part of the beam is taken from a polarisation cube thus allowing saturated absorption spectroscopy along the reference atomic line in an argon discharge cell (0.5 torr, 50 MHz). The second part, more intense, is sent through a single mode fibre to the vacuum chamber.

2.3 Interferometer

The interferometer is placed on a small optical frame inside the vacuum chamber (Fig. 4). Two counter propagating laser beams, about 2 mm in diameter, cross the atomic beam in order to polarise it. A triple μ-metal pot, of cylindrical symmetry, with guiding coils at the entrance and exit, shields the sensitive zone from stray magnetic fields. This shielding also creates, at each of its sides, a Majorana transition region where the direction of the imposed inner and outer tiny magnetic fields varies abruptly by about 90°. As a consequence, the spin rotating at the

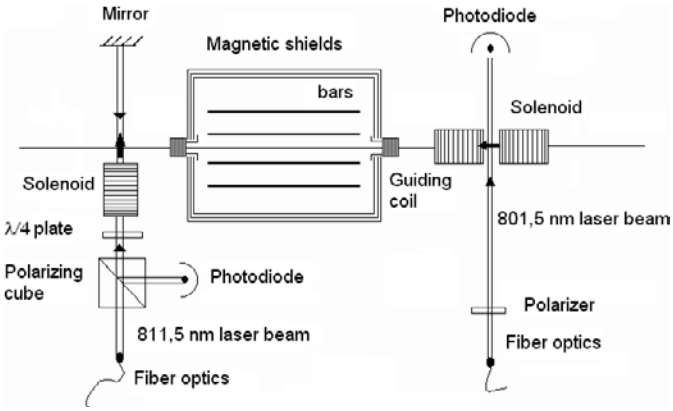

Fig. 4. Scheme of the interferometer. The circularly polarised laser light at $\lambda = 811.5$ nm in a magnetic field transverse with respect to the atom beam (horizontal axis) is used as a polariser ($M = +2$ sublevel, see Fig. 6). A second laser beam at $\lambda = 801.5$ nm, crossing the atom beam at right angle in a longitudinal magnetic field, is used as an analyser ($M = 0$, see Fig. 8). "Guiding" coils set at both ends of the shielded zone allow for the adjustment of the Majorana zone operation (see text). Inside the shielded region (phase object) copper bars supplied with DC currents produce various magnetic field configurations.

Larmor frequency does not adiabatically follow the new direction of the inner magnetic field. In the inside shielding, each atom in a superposition of M states (quantized along the new transverse field direction) evolves in the magnetic field created by a set of copper bars where a current is allowed to flow. There are 8 such copper bars, 5 mm in diameter, 52 mm in length, placed evenly on a 12.5-mm radius circle. When properly supplied by electric DC currents they create a transverse magnetic field. After the exit-guiding coil, the atomic beam is analysed by a second laser. Its quantization axis is defined here by a magnetic field directed along the supersonic beam axis.

The polariser and analyser of the interferometer will be now described in more detail. The Majorana zones and the adiabatic evolution of the atom M states in the triple μ-metal cylinder will be detailed in Section 3.

2.4 Polarisation

To polarise the Ar* $^3P_2$ beam in the Zeeman state $M = +2$, or equivalently $M = -2$ (which leads to an identical interferogram), we use a laser beam frequency connecting the metastable state $J = 2$ to the $J = 3$ ($^3D_3$) upper radiative state. The wavelength of this closed transition is 811.5 nm (Fig. 2). We use circularly polarised light in a standing wave crossing the atomic beam at right angle. This is achieved when the collimated light beam at the fibre output is polarised linearly by a proper polarisation cube, then circularly by a rotatable $\lambda/4$ plate. In the crossing region a uniform magnetic field of 2.3 G is set orthogonal to the atom beam. The light is retro-reflected ($R = 95\%$) and then goes without losses to a calibrated

Table 1. Main characteristics dealing with the two optical transitions used in this experiment. Zeeman frequency shifts (in MHz/G) are given for all allowed transitions between the sub-levels.

Transition		811.531 nm		801.479 nm
Landé factors		$g_i = 1.506$ $g_f = 1.338$	$g_i = 1.506$	$g_f = 1.112$
Linewidth $\Gamma/2\pi$		5.8 MHz	5.6 MHz	
Total decay time		27 ns	29 ns	
Transition decay time		27 ns	104 ns	
Transition probability		100%	28%	
Saturation intensity		1.3 mW/cm^2	4.4 mW/cm^2	
Light polarisation		σ^+		π
Atomic dipolar transition		$\Delta M = +1$		$\Delta M = 0$
Zeeman shift (MHz/G)	from $M = -2$	2.34	2.66	1.10
	from $M = -1$	2.11	2.11	0.55
	from $M = 0$	1.87	1.56	no
	from $M = 1$	1.64	1	-0.55
	from $M = 2$	1.40	no	-1.10

photodiode when the $\lambda/4$ plate sets a circular light fully reflected at the prism. In this configuration, atoms see the same helicity with respect to the quantization axis imposed by the magnetic field. The polarisation process, through the closed transition, does not induce losses in the detected metastable flux. Therefore, to obtain (by means of a metastable flux measurement) an information about the degree of $M = +2$ atomic polarisation, we use the same optical device with the open transition line at 801.5 nm (see Tab. 1) which partly depopulates the $^3P_2$ state. This line connects the metastable state $J = 2$ to the $J = 2$ ($^3D_2$) upper radiative state, which can decay to the ground state *via* the $^3P_1$ and $^1P_1$ radiative levels (Fig. 2). A simplified rate equation formalism whereby the magnetic field is 0 and the laser light polarised circularly predicts a stationary $^3P_{2M=+2}$ metastable flux equal to 0.275 times the initial $^3P_2$ flux, initially distributed evenly in each M states ranging from -2 to $+2$ (statistical mixture) [10]. This result still holds when the interaction takes place in a moderate magnetic field. We checked this point with the Faraday cup detector giving a metastable signal equal to about 40% of the initial flux including the non resonant $^3P_0$ atoms, in agreement with the expected value: $(0.275 \times 5 + 1)/6$. More information can be obtained by measuring the metastable flux. We carried out various scans at a fixed laser power, in a magnetic field varying from negative to positive values. In Figure 5 the depopulation signal obtained with a circular polarisation, under saturation conditions is shown (open circles).

Symmetrical depopulation, with a maximum depletion when the applied magnetic field is 0 indicates (i) a loss of the imposed quantization axis which is replaced by the residual magnetic field, (ii) an optimal tuning of the crossing angle between the laser and the atoms (the Doppler shift is 2 MHz per mrad at 1 650 m/s). We observe a depopulation reaching 60% when the field is around 2.3 G, when the transition is saturated. This demonstrates that this field is high enough to balance the residual earth magnetic field and small enough to stay within the partial width of the line decaying to the metastable state. Pushing effects by the laser are prevented, as observed on the

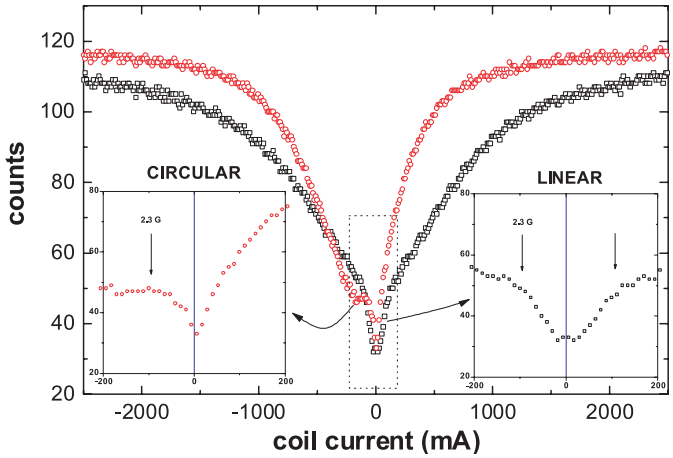

Fig. 5. Depopulation effect induced by a linearly (open squares) and a circularly (open circles) polarised laser light at $\lambda = 801.5$ nm ($^3P_2 \rightarrow {}^3D_2$ open transition) as a function of the applied magnetic field (23 G/A). The laser power saturates in both cases the transition. Ar atoms are seeded in a H_2 nozzle beam (velocity $v = 1\,645$ m/s); insets: zoom on the small-field region. "Counts" correspond to the digitised analogue output of the pico-ammeter.

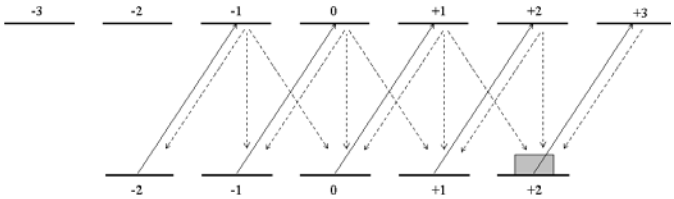

Fig. 6. Polariser: $Ar^*(^3P_2)$ atoms are optically pumped to the $M = +2$ Zeeman sublevel by means of a circularly (σ^+) polarised laser light at $\lambda = 811.5$ nm ($^3P_2 \rightarrow {}^3D_3$ closed transition).

phosphor screen detector, because the laser beam without detuning is retro-reflected. Then the polariser is set back to the other wavelength to realise the full polarisation of the whole $^3P_2$ beam (Fig. 6), as it will be confirmed by the interference patterns.

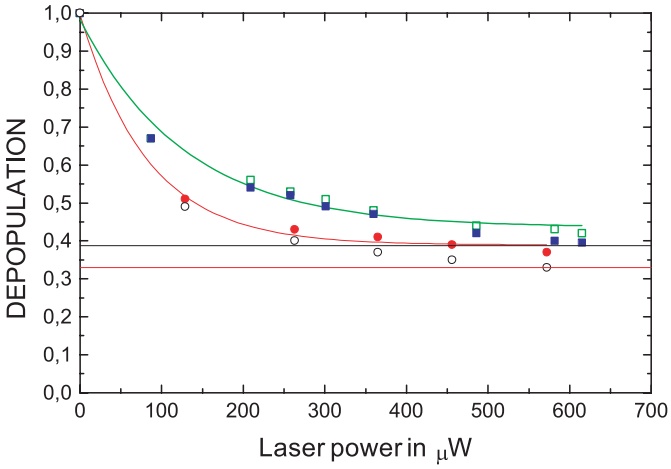

Fig. 7. Analyser: depopulation effect on metastable argon atoms Ar ($^3P_{0,2}$) induced by a linearly polarised laser at $\lambda = 801.5$ nm, as a function of the laser power. Experiment: open circles: $v = 550$ m/s, applied field (referred to the beam direction) +2.3 G; solid circles: $v = 550$ m/s, applied field −2.3 G; open squares: $v = 1\,645$ m/s, applied field: −2.3 G, solid squares: $v = 1\,645$ m/s, applied field +2.3 G. Calculated results are shown as continuous lines. Curve: exponential fit; lower horizontal line: depopulation limit assuming no decay to $^3P_2$, $M = 0$ sublevel; upper horizontal line: depopulation limit including decay to $^3P_2$, $M = 0$. It is observed that depopulation limits for the positive value of the magnetic field are slightly lower than the limits for the negative value. This asymmetry can be explained by a small Doppler shift (laser beam not exactly perpendicular to the atom beam).

2.5 Analysis

The method chosen to analyse the coherent superposition of Zeeman sub-states consists in filtering the $M = 0$ part of it by using the open transition at 801.5 nm. The laser photons do not affect this particular state when a linear polarisation parallel to a magnetic field is applied ($M = 0$, $\Delta J = 0$, $J = 2$ Clebsh Gordan coefficient is zero). On the other hand, all other M states are efficiently depopulated *via* UV emission from the $^3P_1$ and the $^1P_1$ radiative states (Fig. 2).

A numerical calculation shows that the amount of spontaneous emission going to the $M = 0$ state is 0.066 times the $^3P_2$ initial population when the following conditions are fulfilled: (i) the laser interacts with a fully depolarised statistical population of metastable argon atoms in the $^3P_2$ state, (ii) we assume saturation and linear pumping in a zero magnetic field. Different scans have been recorded with the Faraday detector, at different laser intensities in a variable magnetic field. One of them, at saturation is shown in (Fig. 5, open squares).

A Faraday signal ratio with and without the laser (depopulation ratio shown in Fig. 7) is then deduced for a definite magnetic field (2.3 G). As it can be seen saturation conditions are fulfilled even for higher velocities when the laser power is larger than 500 μW. We present also what would be an ideal filtering ratio, *i.e.* without spontaneous emission to the $M = 0$ state. This ratio is 33% including the $^3P_0$ state (1/6 + 1/6). We emphasise that the experimental case when we do interferometry measurements is probably close to the ideal filtering case (shown in Fig. 8), especially in the vicinity of a central bright fringe, where the whole population is in the dark state.

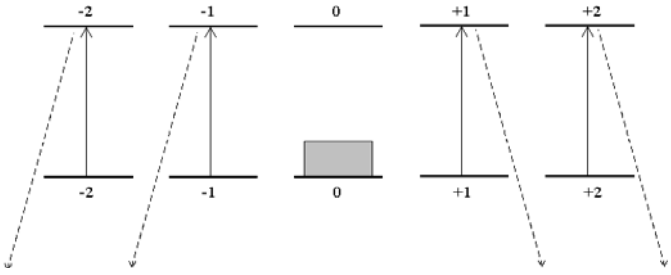

Fig. 8. Analyser: $Ar^*(^3P_2)$ atoms experience a linearly polarised laser light tuned on the open $^3P_2 \rightarrow {}^3D_2$ transition ($\lambda = 801.5$ nm). The only $M = 0$ Zeeman sublevel remains populated in a stationary regime. In this ideal scheme contamination of the $M = 0$ sub-level by spontaneous emission from radiative $M = \pm 1$ levels is ignored.

3 Results and discussion

3.1 Interferometric signal

Let us consider the ideal case of an atom of velocity v, parallel to the symmetry axis of the interferometer (Oz). We simplify also the external motion and consider a plane wave whose wave vector is $\mathbf{k} = m\mathbf{v}/\hbar$. The atom is polarised in the Zeeman state $|J = 2, M = +2\rangle$ in the quantization axis defined by the magnetic field in the laser interaction region. The evolution of the spin is adiabatic, and the field direction before the Majorana transition is Oz, that of the guiding magnetic field just before the shield. The wave function can be written $e^{ikz} \otimes |J = 2, M = 2\rangle_z$. Let us now consider the first Majorana transition where the field direction is going to rotate by 90° around a transverse x-axis. A criterion describing this sudden transition is $\omega_B \gg \omega_L$, where ω_B is the angular velocity of the magnetic field and ω_L the Larmor frequency. This condition is best satisfied when the atom velocity is high and when the residual magnetic field inside the shield is small. We can write (*e.g.* [11]):

$$|J = 2, M\rangle = \sum_{M'} D^{(J=2)}_{M'M}(\alpha, \beta, \gamma)|J = 2, M'\rangle,$$

where M is quantized along (Oz) and M' along the new direction of the inner magnetic field, usually transverse (Oz'). $D^{(J)}$ is the finite rotation matrix for a spin J (also called Wigner matrix), and α, β, γ are the Euler angles of transformation from the old reference frame (x, y, z), to the new one (x', y', z'). In the particular case of a 90° swing, α and γ can be set to zero, and thus we can write:

$$e^{ikz} \otimes |J = 2, M = 2\rangle = e^{ikz} \otimes \sum_{M'} d^2_{M'2}\left(\beta = \frac{\pi}{2}\right)|J = 2, M'\rangle$$

where the matrix elements $d_{M'M}$ are given in [11]. One can write the incoming state explicitly (states J, M will be simply noted from now, M):

$$e^{ikz} \otimes \left(\frac{1}{4}|-2\rangle_{z'} - \frac{1}{2}|-1\rangle_{z'} + \sqrt{\frac{3}{8}}|0\rangle_{z'} - \frac{1}{2}|+1\rangle_{z'} + \frac{1}{4}|+2\rangle_{z'} \right). \quad (1)$$

If we call $\phi_{M'}(z)$ the part of the wave function describing the external motion state of the M' component, then the wave function interacting with a uniform magnetic field along z', localized in the region $[0,\ L]$, is written as a sum of tensorial products of internal and external states:

$$|\Psi_{JM}(z)\rangle = \sum_{M'} \phi_{M'}(z) \otimes |M'\rangle. \quad (2)$$

The time independent Schrödinger equation at energy $E = \hbar^2 k^2/2m$ leads to a set of $2J+1$ uncoupled equations since $|M'\rangle$ is an eigenfunction of the Zeeman operator $V = g\mu_B \mathbf{J}\cdot\mathbf{B} = g\mu_B B(z) J_{z'}$ with the eigenvalue $M' g\mu_B B(z)$. Notice that even in the case of a uniform magnetic field there is a gradient $B(z)$ at both sides of the field, which is responsible for a longitudinal Stern Gerlach effect. Thus we can write for each M':

$$\left[\frac{-\hbar^2}{2m}\Delta + M'\varepsilon(z)\right]\phi_{M'}(z) = E\phi_{M'}(z) \quad (3)$$

where $\varepsilon(z) = g\mu_B B(z)$ is the Zeeman energy for $M' = 1$. Equivalently we can write:

$$[\Delta + K_{M'}(z)]\phi_{M'}(z) = 0 \quad (4)$$

where

$$K_{M'}(z) = \sqrt{\frac{2m}{\hbar^2}(E - V_{M'}(z'))}$$

is the local wave number, and $V_{M'}(z) = M'\varepsilon(z)$ the Zeeman energy for M'.

Because any potential variation $V_{M'}(z)$, at the local wavelength scale $\lambda_{M'}(z) = 2\pi/K_{M'}(z)$, is very small compared to the local kinetic energy, the WKB approximation is widely justified. In our experiment the Ar^* atoms have a velocity of 550 m/s (1 650 m/s when they are seeded in hydrogen) and a narrow velocity distribution ($\delta v/v = 8\%$). Their kinetic energy is about 60 meV. This is a very high value compared to typical Zeeman energies of a few neV. Furthermore, an alternative form of the WKB condition, valid for our problem is:

$$\left|\frac{\mathrm{d}\varepsilon(z)}{\mathrm{d}z}\right| \ll \frac{2\pi E}{\lambda_{\mathrm{dB}}} \text{ where } \lambda_{\mathrm{dB}} = 0.18 \text{ Å (pure Ar)}$$
$$\text{or } 0.06 \text{ Å (Ar seeded in } H_2),$$

corresponding to an upper limit of 2 eV/Å. A consequence of $E \gg |V_{M'}|$ is that, for the calculation, the external motion of the atom can be considered as uniform (and classical): $\mathbf{r}(t) = \mathbf{r}_0 + (t - t_0)\mathbf{v}$, making the effect of $V_{M'}$ be

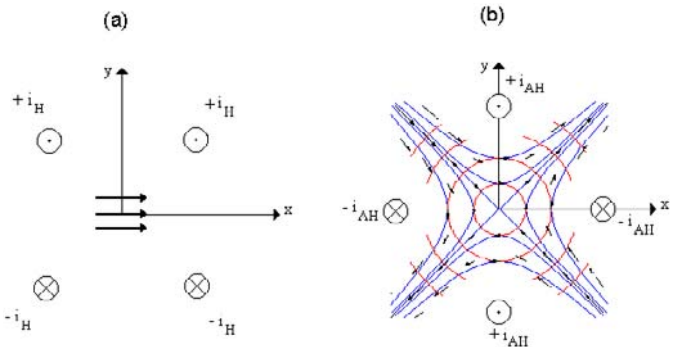

Fig. 9. Magnetic field configurations used in the phase object: (a) homogeneous field ("Helmholtz" configuration) produced in the vicinity of the z-axis by paired currents $\pm i_H$. (b) quadrupolar field ("Helmholtz" configuration) produced by alternate currents $\pm i_{AH}$. Field lines (hyperbolae) and constant-field lines (circles) in the vicinity of the z-axis are shown.

restricted to an action on the internal components (spin) parts of the wave function, incorporating into each $\phi_{M'}(z)$ its own phase-shift $\varphi_{M'} = \int_0^L (K_{M'}(z) - k)\mathrm{d}z$. Using $E \gg \varepsilon(z)$ allows simplifying the phase-shift $\varphi_{M'} = M'\varphi$ in the Glauber form [12] with:

$$\varphi \approx -\frac{1}{\hbar v}\int_0^L \varepsilon(z)\mathrm{d}z. \quad (5)$$

In the case of a uniform magnetic field, named B_H ("Helmholtz" field), created by the current i_H (Fig. 9a), we can write in the vicinity of the z-axis:

$$\mathbf{B}_H = \frac{\sqrt{2}\mu_0}{\pi a} i_H \hat{\mathbf{x}} \quad (6)$$

a is the distance of the bars to the Oz axis and now,

$$\varphi_{M'} = M'\varphi = -M'\frac{g\mu_B}{\hbar}\int_0^L \mathrm{d}z \frac{B_H(r)}{v} \approx -M'\frac{g\mu_B B_H L}{\hbar v}. \quad (7)$$

In the case of a quadrupolar magnetic field, named B_A ("anti-Helmholtz" field) created by the current i_A (Fig. 9b), we can write in the vicinity of the z-axis:

$$\mathbf{B}_A = \frac{2\mu_0}{\pi a^2} i_A \rho \hat{\mathbf{u}} = G\rho\hat{\mathbf{u}} \quad (8)$$

where $\hat{\mathbf{u}}$ is the unit vector along the hyperbolae field lines, G the radial uniform gradient and ρ, the distance between the atom and the z-axis. Then in this case:

$$\varphi_{M'} = M'\varphi = -M'\frac{g\mu_B}{\hbar}\int_0^L \mathrm{d}z \frac{B_A(\rho, z)}{v} \approx -M'\frac{g\mu_B G L}{\hbar v}\rho. \quad (9)$$

Obviously, all atoms having a trajectory parallel to Oz will develop this phase shift. Notice the linear dependence on ρ. For any straight line trajectory, in general not parallel to Oz, owing to the linear dependence of B on ρ,

an expression of the phaseshift similar to (9) is obtained, ρ being replaced by ρ_m, the value of ρ in the mid plane of the phase object. Thus we can express the two different cases, with a common developed phase shift φ and we will distinguish later between the Helmholtz case (v dependent) and the anti-Helmholtz case (v and ρ dependent in this simple model). In the limit of the plane wave, the state of the atom after the interaction with the magnetic field profile becomes factorisable and can be express as follows:

$$\mathrm{e}^{\mathrm{i}kz} \otimes \left(\frac{1}{4}|-2\rangle_{z'} \mathrm{e}^{-2\mathrm{i}\varphi} - \frac{1}{2}|-1\rangle_{z'} \mathrm{e}^{-\mathrm{i}\varphi} + \sqrt{\frac{3}{8}}|0\rangle_{z'} - \frac{1}{2}|+1\rangle_{z'} \mathrm{e}^{+\mathrm{i}\varphi} + \frac{1}{4}|+2\rangle_{z'} \mathrm{e}^{+2\mathrm{i}\varphi} \right) \cdot \quad (10)$$

We consider now a second Majorana transition (90° rotation leading to a new axis opposite to Oz). The signal after the (ideal) analysis of the $M = 0$ spin state is written:

$$\left| \frac{1}{4}\sqrt{\frac{3}{8}} \mathrm{e}^{-2\mathrm{i}\varphi} - \frac{1}{4}\sqrt{\frac{3}{2}} + \frac{1}{4}\sqrt{\frac{3}{8}} \mathrm{e}^{+2\mathrm{i}\varphi} \right|^2 = \frac{3}{64}(3 - 4\cos 2\varphi + \cos 4\varphi) = \frac{3}{8}\sin^4 \varphi \cdot \quad (11)$$

One may notice because of this special exit Wigner rotation that terms $\mathrm{e}^{\pm \mathrm{i}\varphi}$ are absent, giving an unambiguous π period to the interferential function.

This is the general form of the expected signal, in the present polarisation scheme (polariser $M = +2$, analyser $M = 0$). Here, the central fringe is a dark one. Similar expressions are easily derived for all other possible schemes.

3.2 Experiment with a transverse uniform field

A current i_H is scanned among 4 bars in order to obtain a homogeneous field through the whole $\mathrm{Ar}^*(\mathrm{H}_2)$ beam (Fig. 9a). Fast Ar^* atoms ($v = 1\,650$ m/s) have been preferred to thermal ones ($v = 550$ m/s) because of some difficulties to handle the Majorana transitions and the inner residual field. Nevertheless, interference patterns have also been obtained with slow atoms. However the central fringe and the fringe period do not fully agree with simple theoretical predictions.

We emphasise here that the whole beam is detected. At the Faraday plate we record the analog output of the pico-ammeter, converted to digital counts through a time-to-frequency converter. The signal is then sent *via* a multi channel analyser card to our computer. The following signals are recorded:

(i) the signal without lasers,
(ii) the signal with polariser and analyser,
(iii) the signal without polariser and with analyser,
(iv) the background signal (the Faraday plate is set out of the beam).

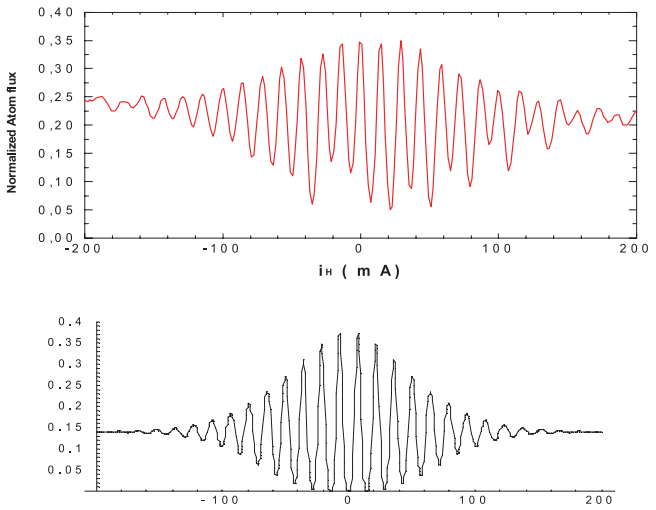

Fig. 10. Interference pattern obtained in the Helmholtz configuration, using the Faraday-plate detector, by scanning the current i_H (1 mA correspond to 0.45 mG). The (constant) contribution of $^3\mathrm{P}_0$ atoms and the background signal are substracted. The signal is normalised with respect to the total incident metastable flux. The lower part of the figure shows the calculated pattern.

It is then possible to normalise our interferogram (Fig. 10) with respect to the amount of polarised interfering atoms. Comparison with a theoretical ideal signal is given. Each scan is of 40 s duration, and we carried out 10 pass counts. We remark a good general behaviour in the number of visible fringes. We count about 21 fringes at a full 300 mA range, making thus a fringe interval of about 14.28 mA. The field generated by 4 bars has been calculated *in vacuo* (0.50 mG/mA). It gives a similar total number of visible fringes in the 300 mA range making a fringe interval of 16.6 mA. It is likely that this small discrepancy is due to the presence of the high permittivity μ-metal inner shielding (radius 20 mm), making appear image bars that increase the field by a factor 1.4 for an infinitely thick wall, and a smaller factor for the present finite thickness of the material (1 mm). Although, the experiment provides unambiguously the right interfringe, in our case the smallest possible one as predicted by formula (11).

The maximum amplitude of fringes in the experimental normalised pattern is 0.30, to be compared with the theoretical value 0.375. The constant limit of the interferogram towards high interference orders is experimentally 0.23 instead of the theoretical value $9/64 \approx 0.14$. The central dark fringe ($\varphi = 0$) should theoretically give a zero signal value while experimentally it is about 0.05. This corresponds to a lack of about 20% in contrast. Nevertheless this is in reasonably good agreement with the calculation since this latter assumes ideal polarisation processes. In particular in the ideal analysis process the selection of the $M = 0$ sub-state is assumed. Actually this state is also populated by spontaneous emission from other upper sublevels the populations of which depend on the phase-shift in the interferometer.

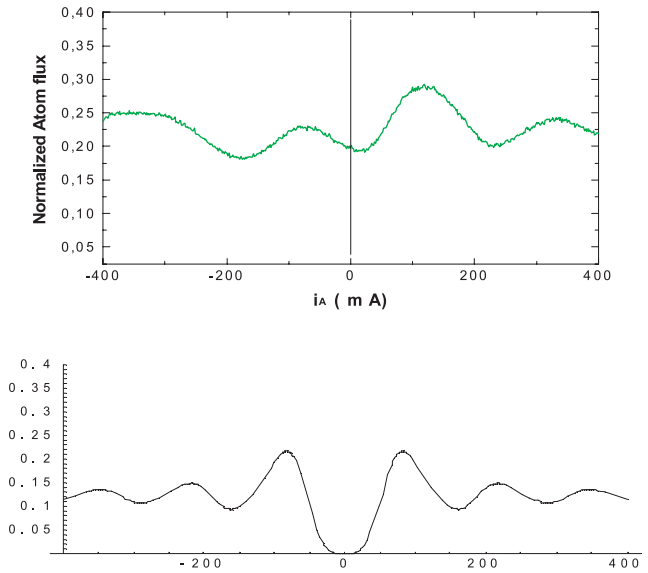

Fig. 11. Same as Figure 10 in the anti-Helmholtz configuration (quadrupolar field), by scanning the current i_A (the gradient G is 51 mG/mm/A). The lower part shows the calculated pattern.

Another discrepancy is seen in the shape of the fringes themselves, which exhibits a slight asymmetry with respect to the sign of i_H. This effect can be attributed to an imperfect operation of the Majorana zones which cannot be exactly described by a simple $\pi/2$ rotation.

3.3 Experiment with a radial gradient field

In a second scan of current i_A (Fig. 9b) we create a quadrupolar field through the whole $Ar^*(H_2)$ beam (Fig. 11). Notice a slower modulation than in the previous Helmholtz case. The discrepancies already noticed in the Helmholtz case are enhanced here, which can be explained by the use of a quadrupolar magnetic field.

Then we remove the Faraday plate from the beam in order to use the position sensitive detector. In a first step, the Gaussian atomic beam profile (without the interferometer) is centred on the detector. When the interferometer and its two diaphragms (2 mm in diameter) is positioned, the resulting profile appears slightly shifted (by about 2.5 mrad) in the laboratory horizontal direction (vertical direction in the figures). This explains why the profile observed with no field in the interferometer is not Gaussian (see the first image in the series of Fig. 12).

In a first series we use gradients (51 mG/mm/A) increasing by steps (Fig. 12). The expected interference patterns, namely a central dark hole surrounded by annular fringes is observed. The whole pattern is more and more compressed as the gradient is increased. Notice the fixed position of the central fringe. It shows the good coincidence of the magnetic and the collimation axes of the interferometer. At the maximum value of the gradient used (20 mG/mm) the diameter of the hole (150 μm) approaches the finite resolution of the detector.

In a second series, an increasing homogeneous field $\mathbf{B}_H$ is added to the quadrupolar field (Fig. 13). As expected the whole interference pattern is translated. Due to the fact that the homogeneous field is produced by bars set at 45° from the "i_A bars", this translation is directed perpendicularly to the "Helmholtz field" direction. Obviously, at large enough values of i_H the central hole gets out of the field of detection insofar as the zero field line gets out of the beam inside the interferometer. Notice that the remaining part of the annular fringes have opposite concavities according to the sense of the translation.

A high sensitivity of these images to the misalignment (offset of the source point and polar angles of the mean velocity axis) of the supersonic beam with the magnetic axis has been observed. For a single value of the gradient and two slightly different positions of the beam impact on the detector, *e.g.* with a 4 mm shift, dramatic changes in the interference patterns are observed, in agreement with a simple simulation.

4 Conclusion

In this work, we have demonstrated the feasibility of a Stern Gerlach interferometer operating with a supersonic beam of Ar^* atoms. Laser diodes have successfully been used to polarise ($M = +2$) and to analyse ($M = 0$), a $^3P_2$ Ar^* atom beam. Global detection of the interference signal has been done with a Faraday plate detector connected to a pico-ammeter. Typical fluxes are in the range of 10^{10} atoms/s, thus giving precise interferograms obtained with acquisition times of the order of one minute.

The high internal energy (≈11.5 eV) of metastable Ar^* atoms, allows a position-sensitive detection by means of a micro-channel-plate detector followed by a phosphor screen. The ultimate resolution of the detector is 50 μm, the distance between two adjacent channel axes. This corresponds to a width of about 13 μm in the mid plane of the interferometer. An external CCD camera used for the first time in Stern Gerlach interferometry shows the possibility of modulating the transverse profile of the atomic beam by an interference pattern, here a central dark spot surrounded by annular fringes. This has been done in an immaterial way, by simply using a quadrupolar magnetic field at the heart of the interferometer. It has also been demonstrated that the addition of a homogeneous field allows a translation of the pattern as a whole in any transverse direction and by a controlled amount. Atomic-polarisation schemes different from the present one are feasible as well. In particular it is rather easy to pass from a central dark fringe to a bright one, which provides us with an atomic spot that can be displaced at will in the transverse plane. A key point in the experiment using a nozzle-beam with a narrow angular distribution is the quality of the alignment of the beam axis with the magnetic symmetry axis, an alignment to which the resulting modulated profiles are very sensitive.

In the near future, experiments using a central bright peak are planned in order to investigate which ultimate spot size is achievable by increasing the magnitude of the

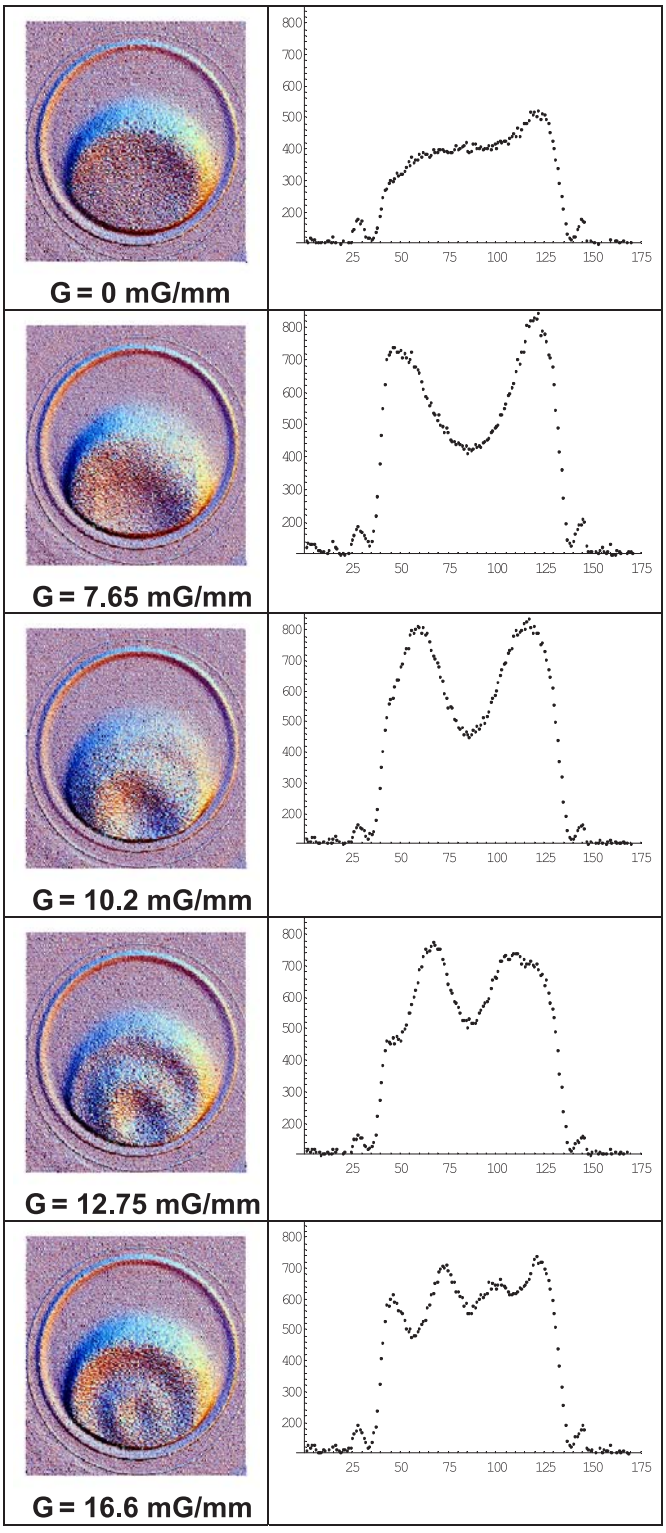

Fig. 12. Left panel: beam profiles recorded by the camera (transverse axes x, y), for increasing values of the gradient. Values of the gradient G are indicated (in mG/mm). The scale is given by the outer circle which is the border of the phosphor screen (diameter 10 mm, corresponding to 2.4 mm in the mid plane of the interferometer). Right panel: sections of these profiles (counting rate as a function of camera pixel number) by the horizontal line passing through the centre of the pattern.

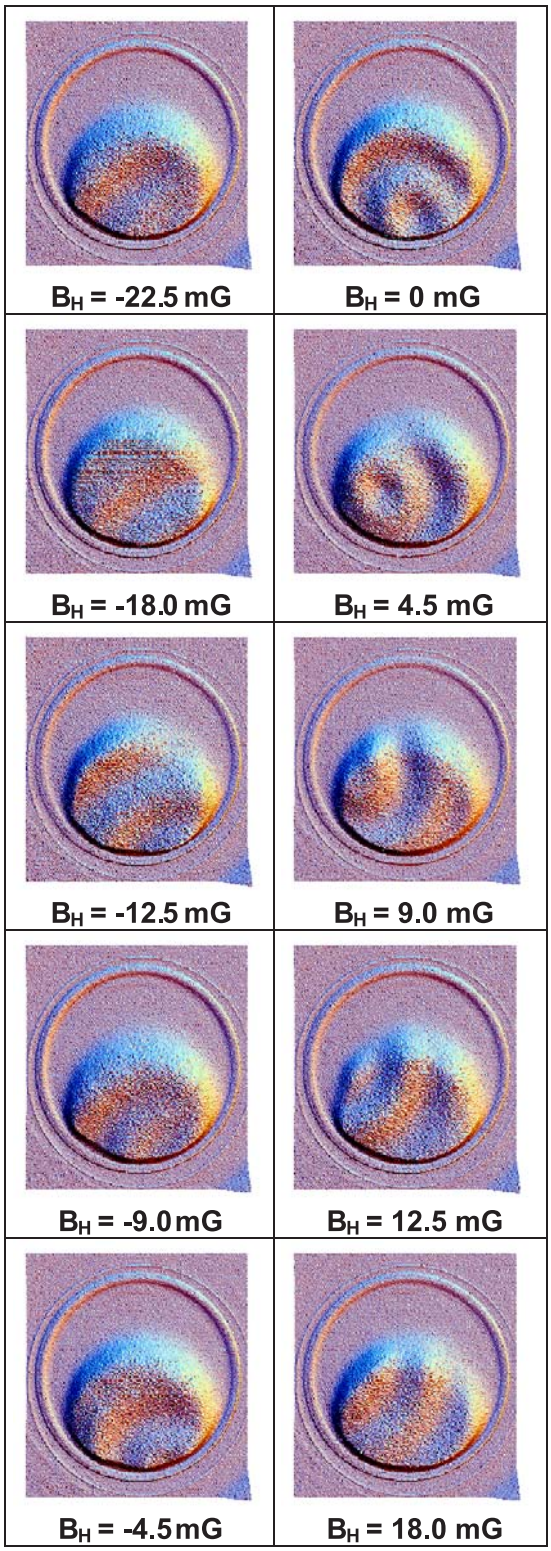

Fig. 13. Beam profiles recorded at a fixed value of the gradient ($G = 12.75$ mG/mm), an homogeneous field (B_H) being added to the quadrupolar field, to produce a translation of the interference pattern as a whole, in a direction making an angle $\pi/8$ (downwards) with the horizontal direction. Algebraic values of B_H are indicated (in mG). One may notice the opposite concavities of the remaining annular fringes at both ends of the scan.

gradient. In principle, owing to the low values of the gradient used so far ($G \leq 20$ mG/mm) quite large reduction factors should be obtained. Nevertheless, in such experiments several criteria must be fulfilled: (i) a good superposition of the beam and the magnetic axes; (ii) a good spatial resolution of the position sensitive detector (<1 μm); (iii) the atomic wave packets splitted out by the intense magnetic gradient should overlap in order to preserve their interference; indeed there exists as the distance of observation becomes larger and larger, a competition between the natural (hyperbolic) spreading of the wave packets and the (linear) Stern Gerlach deflection. While they need delicate instrumental improvements, the realisation of these criteria appears quite achievable. Beyond this step, this device could be used as a versatile optical element in what concerns: (i) micro-probing of surfaces, (ii) atomic lithography, (iii) realisation of new atomic sources for fundamental interactions studies.

We thank Dr. Michèle Leduc from the Laboratoire Kastler-Brossel (Paris), for kindly lending us a CCD camera, which has permitted to directly record the beam profiles. We thank B. Cardin who efficiently helped us in the experiment. One of us (M.B.) thanks the Fondation/Institut Louis de Broglie for providing him with a financial support. Another one of us (T.D.) is a post-doctoral fellow of the Flemish Fund for Scientific Research. This work has been partly supported by ANVAR contract Nr. A00 09334QAFAT.

References

1. B.G. Englert, J. Schwinger, M.O. Scully, Found. Phys. **18**, 1045 (1988); J. Schwinger, M.O. Scully, B.G. Englert, Z. Phys. D: At. Mol. Clust. **10**, 135 (1988)
2. M. Bloom, K. Erdman, Can. J. Phys. **40**, 179 (1962)
3. S. Cruz-Barrios, J. Gómez-Camacho, Phys. Rev. A **63**, 012101 (2000)
4. M. Boustimi, V. Bocvarski, B. Viaris de Lesegno, K. Brodski, F. Perales, J. Baudon, J. Robert, Phys. Rev. A **61**, 33602 (2000)
5. E. Rasel, F. Pereira Dos Santos, F. Saverio Pavone, F. Perales, C.S. Unnikrishnan, M. Leduc, Eur. Phys. J. D **7**, 311 (1999)
6. J. Robert, Ch. Miniatura, S. Nic Chormaic, J. Lawson-Daku, O. Gorceix, F. Perales, J. Baudon, J. Phys. II France **4**, 2061 (1994); B. Viaris de Lesegno, M. Boustimi, J.Ch. Karam, F. Perales, J. Reinhardt, J. Baudon, J. Robert, Ann. Fond. Louis de Broglie **26**, 571 (2001)
7. E. Majorana, Nuovo Cim. **9**, 43 (1932)
8. B. Viaris de Lesegno, thèse de doctorat, Université Paris 13, France, 2000
9. B. Brutchy, H. Haberland, Phys. Rev. A **19**, 2232 (1979)
10. The stationary solution can be expressed with P, the probability to return to the metastable state as: $(P^2 - 0.6P + 3.6)/[(2-P)(3-P)]^2$. Evidently, if $P = 1$, the result is 1
11. L. Landau, E. Lifchitz, *Quantum Mechanic* (Ed. Mir, Moscow, 1974)
12. R.J. Glauber, *Lectures in theoretical physics* (Interscience, New-York, 1959), Vol. 1